ACS APPLIED MATERIALS & INTERFACES

Research Article

www.acsami.org

Enhanced Photocatalytic Performance of the Graphene-V_2O_5 Nanocomposite in the Degradation of Methylene Blue Dye under Direct Sunlight

Mahalingam Shanmugam,[†] Ali Alsalme,[‡] Abdulaziz Alghamdi,[‡] and Ramasamy Jayavel*[,†]

[†]Centre for Nanoscience and Technology, Anna University, Chennai, Tamil Nadu 600 025, India

[‡]Department of Chemistry, College of Science, King Saud University, P.O. Box 2455, Riyadh, Riyadh Province 11451, Saudi Arabia

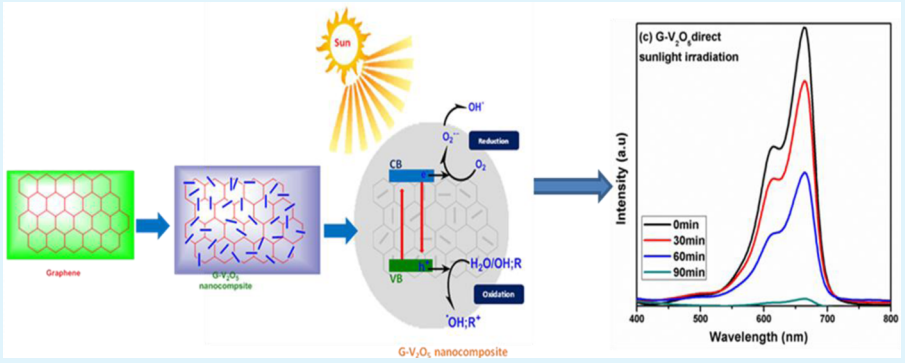

ABSTRACT: A simple and efficient solution mixing method has been developed for the synthesis of the G-V_2O_5 nanocomposite. By this method, one-dimensional V_2O_5 rods are decorated onto the two-dimensional graphene sheets. The synthesized nanocomposites are characterized by XRD, SEM with elemental mapping, TEM, FT-IR, Raman, BET, and XPS analyses. The photocatalytic activity of the G-V_2O_5 nanocomposite studied with methylene blue dye shows strong degradation efficiency with direct sunlight irradiation compared to UV and visible light sources. The mechanism of methylene blue dye degradation by the G-V_2O_5 nanocomposite has been elucidated through the kinetics of the degradation process by calculating the rate constant and half-life time of the degradation process.

KEYWORDS: *graphene, V_2O_5, nanocomposite, simple solution mixing, photocatalytic MB dye degradation, sunlight irradiation*

INTRODUCTION

Environmental pollution is one of the greatest problems in the recent past. The level of pollutant is increasing every year, causing grave and irreparable damage to the globe from the surface to the core. The industrial effluent is identified as the primary source of water contamination, which leads to the soil pollution. The photocatalytic degradation is an important process of wastewater treatment, capable of removing harmful heavy organic contaminations.[1] It has several advantages like low cost, complete mineralization, and low temperature process.[2] The nanosized metal oxide and metal oxide nanocomposites have been reported as good photocatalytic materials with extended surface area and recyclability.[3] Carbon based materials combined with metal oxides are known to have improved photocatalytic activity. Activated carbon and carbon nanotubes have been investigated to control the resistivity of V_2O_5 rods.[4,5] Graphene, the 2D structure of sp^2-bonded carbon atoms arranged in a honeycomb lattice, was first isolated from 3D graphite by mechanical exfoliation.[6] It has also been reported that the graphene-metal oxide composite possesses good photocatalytic activity, compared to the pure metal oxide.[7−14]

The transition metal oxides such as V_2O_5 and VO_2 have received great attention, due to their outstanding properties in support of diverse significant applications.[15] Currently different metal oxide based photocatalysts are used for solar hydrogen production, although the efficiency was relatively low.[16] V_2O_5 is a strong metal oxide catalyst with low band gap (2.2 eV), and its composite with graphene sheets possesses strong photocatalytic activity. With lower band gap, V_2O_5 has an efficient photocatalytic activity under visible light without any dopants, in addition to the strong photocatalytic properties under visible light irradiations.[17] Within the scope of our literature survey, only a few reports are available on the G-V_2O_5 nanocomposite, and the preparation method has been reported to be complex.[18,19] Recently, we have fabricated the G-V_2O_5 nanocomposite with electrospun V_2O_5 nanofibers.[20] The resultant composite exhibits residual stress due the difference in thermal expansion mismatch between graphene oxide and V_2O_5 because of the high aspect ratio of the fiber.

Received: April 28, 2015
Accepted: June 22, 2015
Published: June 22, 2015

DOI: 10.1021/acsami.5b02715
ACS Appl. Mater. Interfaces 2015, 7, 14905−14911

In the present investigation, the G-V_2O_5 nanocomposite has been synthesized by a simple and efficient solution mixing method with hydrothermally grown V_2O_5 one-dimensional structures. The V_2O_5 rods are decorated onto the graphene sheets. The structural and optical properties were studied by various techniques. The photocatalytic degradation efficiency was analyzed with methylene blue (MB) dye under UV, visible, and direct sunlight irradiations. The prepared nanocomposite has a higher photocatalytic efficiency compared to pure V_2O_5 rods. Among the various irradiation sources, direct sunlight irradiation shows strong degradation. The kinetics of the degradation process have also been studied by calculating the rate constant and half-life time of the degradation process.

EXPERIMENTAL PROCEDURE

Materials and Methods. Graphite powder (Alfa Aesar 99.999% USA), $NaNO_3$ (Merck), $KMnO_4$ SRL (Extra pure AR), H_2SO_4 (Merck 98%, GR Pro Analysis), Millipore water, H_2O_2 (Merck, 30% GR Pro Analysis), HCl (Merck, 35% GR Pro Analysis), and ammonium metavanadate (NH_4VO_3) (Sigma-Aldrich) were used for the material synthesis. The crystalline phase was identified by powder X-ray diffraction (XRD) analysis using CuKα radiation (Rigaku, MiniFlex II-C, Japan). The FTIR spectra were recorded by the KBr pellet method using an Alpha Bruker FT-IR spectrometer (Bruker Optics Systems, Germany). SEM images were recorded using TESCAN, VEGA3SEM (Czech Republic). High resolution TEM images and a Selected Area Electron Diffraction (SEAD) pattern of the composite were recorded using a JEOL 3010 transmission electron microscope. The binding energy and chemical composition of the prepared material were studied by XPS analysis using a Shimadzu, ESCA 3400 X-ray photoelectron spectrometer. Raman spectra were recorded with a Lab RAM HR micro Raman system (France), using He–Ne laser of 632 nm wavelength. A mercury lamp (wavelength of 400 nm) and a UV lamp (wavelength of 365 nm) attached to a UV-chamber (Model No. LABPRO-167) were used as the visible and UV light sources for the irradiation studies. The photocatalytic performance was studied using a UV–vis spectrophotometer.

Reduction of Graphene Oxide to Graphene. Graphene oxide (GO) was synthesized by the Modified Hummer's method as reported earlier.[21] The graphene oxide was reduced to graphene by the chemical reduction method. Graphene oxide (200 mg) was dispersed in 100 mL of Millipore water, and the suspension was ultrasonicated for 1 h. The graphene oxide solution was taken in a three neck round-bottom flask and heated to 100 °C in an oil bath, and 2 mL of hydrazine hydrate was added to the solution with constant stirring for 24 h. By this process the graphene oxide was reduced to graphene as a black powder. The black powder was filtered and washed several times with water and ethanol to remove the unwanted impurities if any. The washed black graphene was dried in a vacuum oven at 60 °C overnight.

Synthesis of G-V_2O_5 Nanocomposites. The V_2O_5 rods were synthesized by the hydrothermal method.[22] The G-V_2O_5 composite was prepared by solution mixing followed by sonication. This method is simple and cost-effective with rapid synthesis compared to the *in situ* method. Schematic representation of the formation of the G-V_2O_5 nanocomposite is shown in Figure 1. In this method, graphene (100 mg) was suspended in 100 mL of water and ultrasonicated for 1 h, followed by constant stirring. 50 mg of V_2O_5 rods was suspended in 50 mL of H_2O, and then the solution was ultrasonicated for 30 min. The prepared V_2O_5 solution was mixed with the graphene solution and stirred for 2 h. After stirring, the solution was filtered and washed several times with H_2O and ethanol. The solid product was dried overnight in a vacuum oven at 60 °C to obtain the G-V_2O_5 nanocomposite.

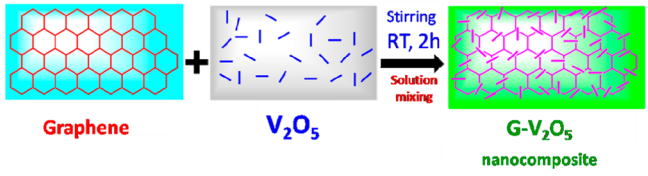

Figure 1. Schematic representation of the formation of the G-V_2O_5 nanocomposite.

Photocatalytic Activity of the G-V_2O_5 Nanocomposite. Methylene blue (MB) dye was used to study the photocatalytic activity of the synthesized G-V_2O_5 nanocomposite. The G-V_2O_5 nanocomposite (10 mg) was dispersed in 50 mL of MB dye solution and maintained at constant stirring in a dark room for 30 min for the adsorption–desorption of the dye molecules. Then the suspended solution was irradiated by UV, visible, and sunlight sources for different time intervals. All the experiments were conducted in a similar environment at the stable temperature of 35 °C. The absorption of 3 mL of the irradiated G-V_2O_5 nanocomposite solution of 3 mL was studied using the UV–visible spectrophotometer.

RESULTS AND DISCUSSION

Structural Analysis. Figure 2 shows the XRD patterns of graphene, V_2O_5, and the G-V_2O_5 nanocomposite. The pattern

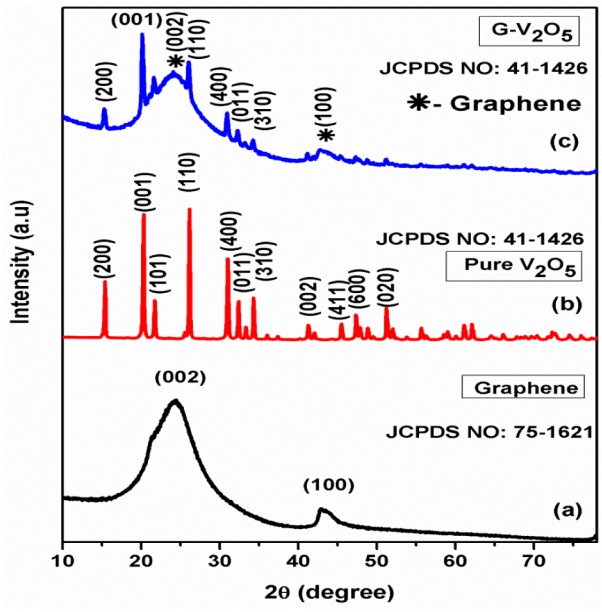

Figure 2. XRD patterns of (a) graphene, (b) V_2O_5 rods with the orthorhombic phase, and (c) the G-V_2O_5 nanocomposite with the hexagonal structure. All peaks are indexed with the corresponding JCPDS values.

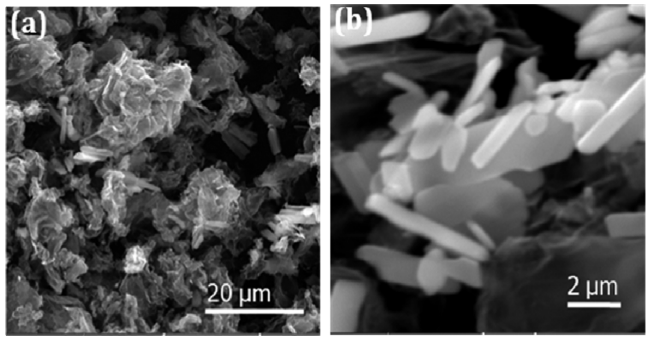

Figure 3. SEM images of (a and b) the G-V_2O_5 nanocomposite with different magnification confirming the uniform distribution of the V_2O_5 rods on the graphene surface.

DOI: 10.1021/acsami.5b02715
ACS Appl. Mater. Interfaces 2015, 7, 14905–14911

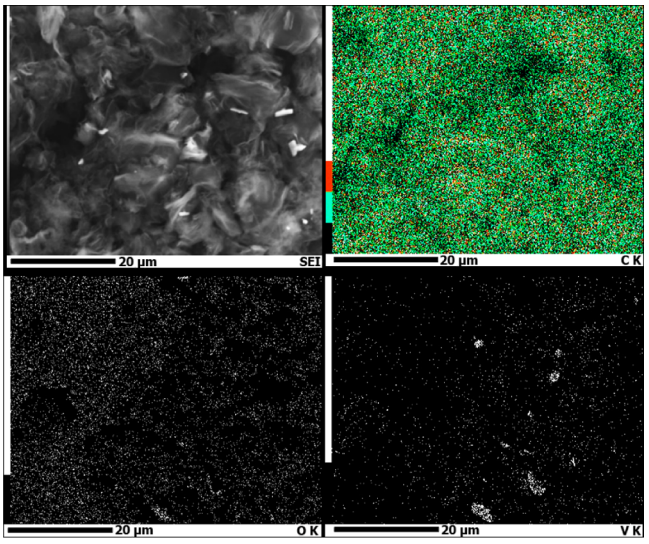

Figure 4. Elemental mapping of the G-V_2O_5 nanocomposite showing the uniform distribution of carbon, oxygen, and vanadium.

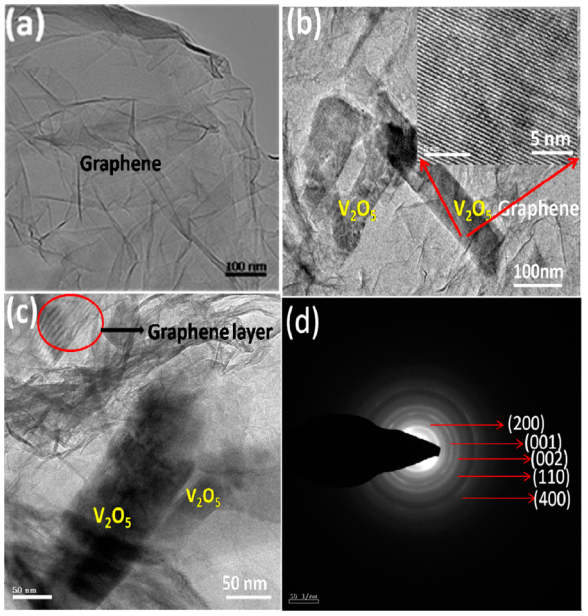

Figure 5. HR-TEM images of (a) graphene, (b, c) the graphene-V_2O_5 nanocomposite, and (d) the SAED pattern of G-V_2O_5.

for graphene shows two prominent peaks (Figure 2 (a)) at an angle of 2θ = 24.43 and 43.14, which are matching with JCPDS No: 75-1621. The diffraction pattern has no other peaks confirming that the hydroxyl and carboxyl groups were completely removed. After the reduction process, (002) and (100) planes of the hexagonal structure of the sp^2-bonded carbon were observed. The broad and low intensity peaks in the diffraction pattern of graphene are due to the poor crystalline nature of carbon. On the other hand, the diffraction pattern of V_2O_5 rods (Figure 2b) confirmed the higher order crystalline nature with the orthorhombic structure. From the diffraction pattern of the G-V_2O_5 nanocomposite, it is observed that the peak intensity of V_2O_5 rods in the graphene sheets was less than that of pure V_2O_5 rods (Figure 2c). The V_2O_5 rods might be distributed uniformly on graphene sheets or incorporated between the sheets.

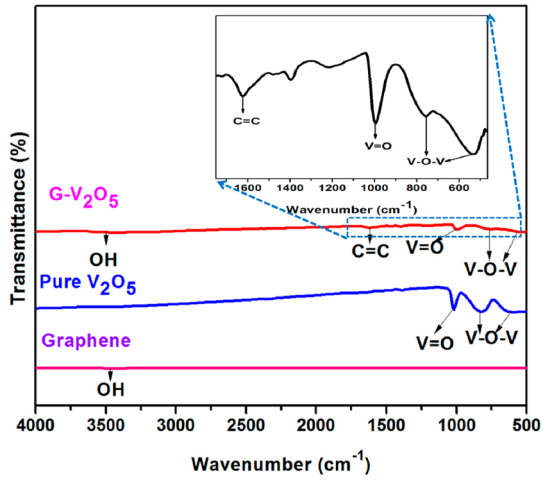

Figure 6. FT-IR spectra of graphene, V_2O_5 rods, and the G-V_2O_5 nanocomposite.

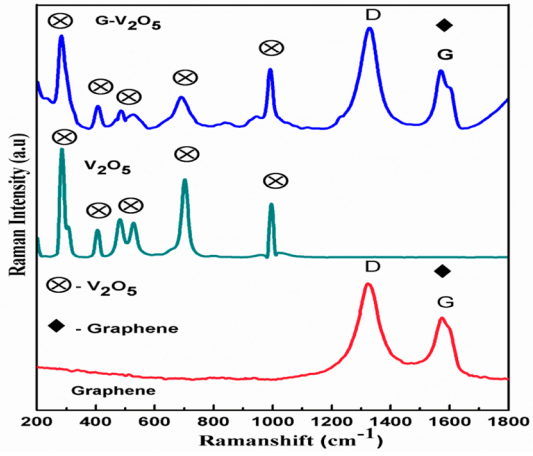

Figure 7. Raman spectra of (a) graphene, (b) V_2O_5 rods, and (c) the G-V_2O_5 nanocomposite.

Morphology Studies. Figure 3(a) shows the SEM image of the G-V_2O_5 nanocomposite at a lower magnification. The image clearly shows the attachment of V_2O_5 rods on graphene sheets. The higher magnification image (Figure 3b) shows the V_2O_5 rods and sheets-like morphology of the G-V_2O_5 nanocomposite. From these images, it is observed that V_2O_5 rods are decorated on the graphene sheets. Figure 4 shows the elemental mapping of the G-V_2O_5 nanocomposite. The composite is carbon rich with the uniform distribution of carbon, oxygen, and vanadium.

TEM Analysis. Figure 5 shows the HR-TEM images of graphene and the G-V_2O_5 nanocomposite. A layered region of graphene with a few layers is shown in Figure 5(a). The higher magnification image clearly shows the folded and layered region of graphene,V_2O_5 rods in Figure 5 (b), and the inset of Figure 5 (b) shows the HRTEM image of V_2O_5 rods with a clear lattice fringe pattern, which confirms the high crystalline nature of V_2O_5. Figure 5(c) shows the incorporation of V_2O_5 rods in the composite. During the sonication process, the graphene sheets and V_2O_5 rods are highly dispersed in the solution medium. The V_2O_5 rods are adsorbed on the surface of graphene sheets during the solution mixing process under stirring conditions. Moreover, the COOH groups and the hydroxyl groups of graphene interact with the V_2O_5 rods and form physical

DOI: 10.1021/acsami.5b02715
ACS Appl. Mater. Interfaces 2015, 7, 14905−14911

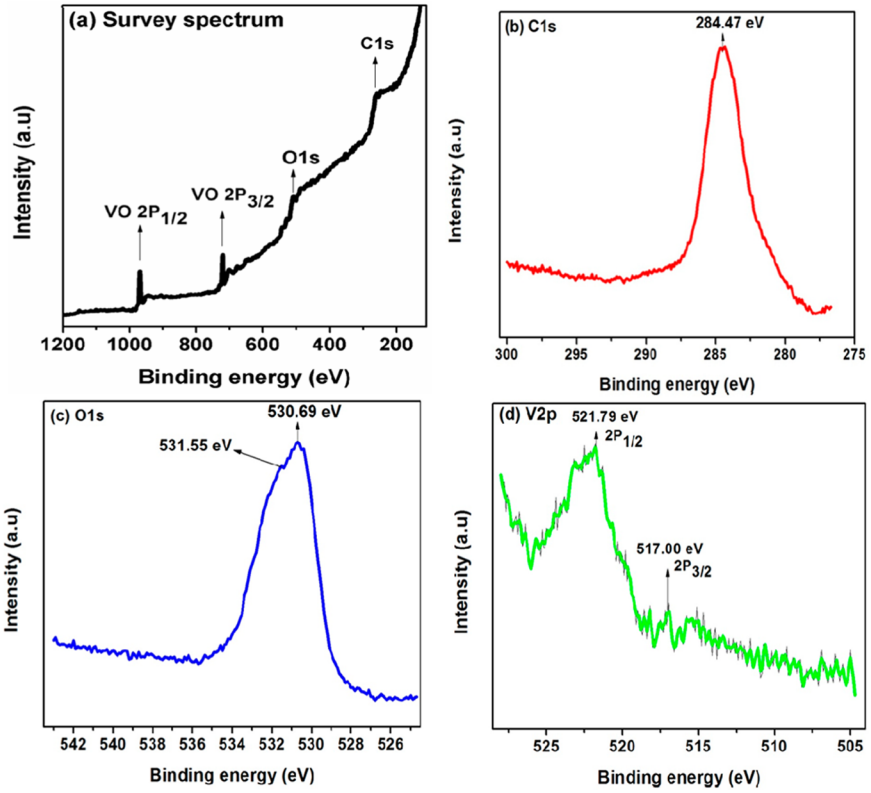

Figure 8. XPS spectrum of the G-V_2O_5 nanocomposite (a) survey spectrum, (b) C 1s spectrum of carbon, (c) O 1s spectrum of oxygen, and (d) V 2p.

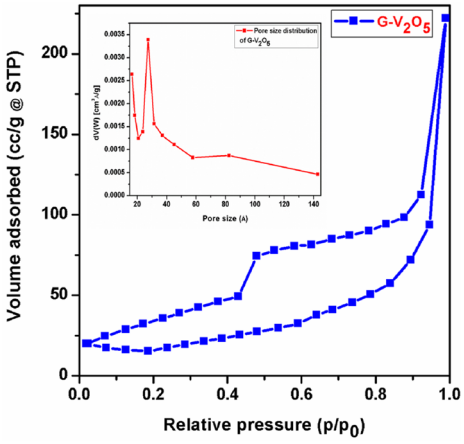

Figure 9. Nitrogen adsorption−desorption of G-V_2O_5 nanocomposites at 77 K.

bonding between them. Figure 5(d) shows the SAED pattern of the G-V_2O_5 nanocomposite, which demonstrates the polycrystalline nature of the composite, and the rings are indexed to the orthorhombic structure.

FT-IR Analysis. Figure 6 shows the FT-IR spectra, which reveal that the graphene oxide was successfully reduced to graphene with hydroxyl, carboxyl, and epoxy groups fully removed except for the C═C sp^2 bonded carbon aromatic ring. The FT-IR spectrum of pure V_2O_5 rods confirms the presence of the V═O stretching mode at 1021 cm^{-1} and the V−O−V stretching mode at 825 and 610 cm^{-1}.[23] On the other hand, the FT-IR spectrum of the G-V_2O_5 nanocomposite shows the band at 1618 cm^{-1} due to the C═C sp^2 bonded carbon aromatic ring and the band observed at 993, 767, and 573 cm^{-1} are due to V═O and V−O−V stretching vibration.[24] The bands observed for the G-V_2O_5 nanocomposite confirmed that the structure is significantly different from pure V_2O_5 rods, and the bands are shifted to a lower wavenumber. The band shift toward the lower energy region indicates the strong interaction between graphene and V_2O_5 rods.

Raman Spectral Analysis. Figure 7 shows Raman spectrum of graphene the Stokes phonon energy shift and the laser excitation creates two main band structures. The band at 1334 cm^{-1} is a primary in-plane vibrational mode of the D-band. The second-order overtone of a different in-plane vibration of sp^2 hybridization of the carbon atom in the graphene sheet is observed at 1581 cm^{-1} called the G-band. The two bands revealed that the D-band is the edge disordered band structure of k-point phonon of A_{1g} symmetry carbon atoms and the G-band is the E_{2g} mode of order band structure of sp^2 hybridization of carbon atoms.[25] The disorder nature of graphene increases, as the Raman intensity increases.[26] From the Raman spectra the defects were related to the I_D/I_G ratio, the intensity of the peaks. For the G-V_2O_5 nanocomposite the ratio is calculated to be 1.84, which reveals that the nanocomposite has fewer defects. The Raman spectrum of pure V_2O_5 rods reveals that the peaks at 286, 410, 484, 534, 704, and 998 cm^{-1} are related to the distinct vibrational modes of the orthorhombic V_2O_5 rods. The strong peak at 286 cm^{-1} is ascribed to the skeleton vibration, and the fine peak at 998 cm^{-1} corresponds to the stretching vibration of the vanadium particle attached to the oxygen atom during the double bond, due to the layered structure of V_2O_5.[27] The Raman spectrum of the G-V_2O_5 nanocomposite revealed that the V_2O_5 rods are attached to the graphene sheets with peaks at 286, 409, 486, 531, 690, and 995 cm^{-1}. The graphene peaks are observed at

DOI: 10.1021/acsami.5b02715
ACS Appl. Mater. Interfaces 2015, 7, 14905−14911

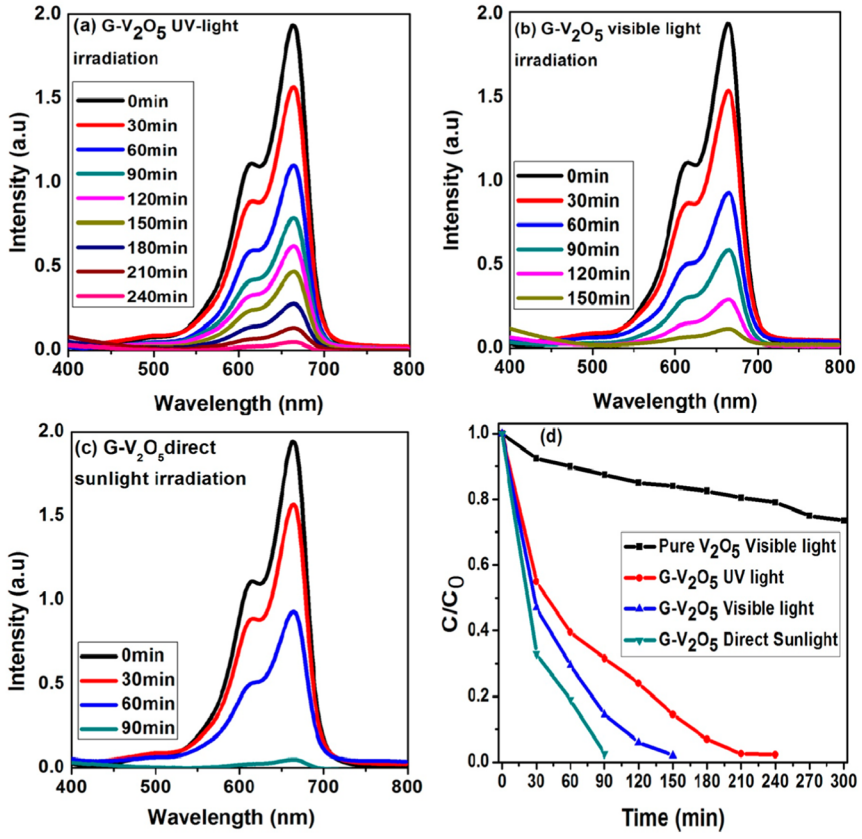

Figure 10. Photodegradation of MB dye under the irradiation of (a) UV-light, (b) visible light, (c) direct sunlight, and (d) C/C_0 vs time (min) for the G-V_2O_5 nanocomposite.

Table 1. Comparison of Rate Constant and Reaction Half-Life Time for Different Irradiation Sources

irradiation source	rate constant, k (h^{-1})	$t_{(1/2)}$ (h)
UV light	0.94 ± 0.047	0.737234
visible light	1.54 ± 0.077	0.45
sunlight	2.2 ± 0.11	0.315

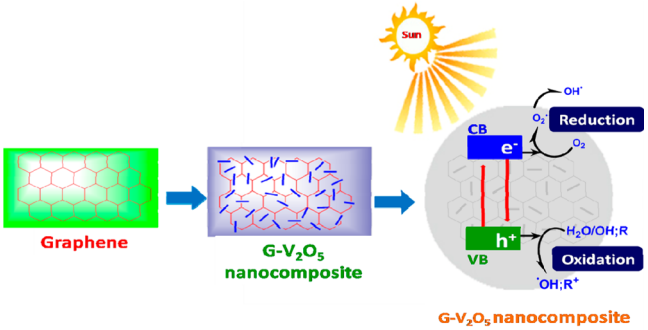

Figure 11. Mechanism of photodegradation of MB dye molecule due to the G-V_2O_5 nanocomposite under sunlight irradiation.

1581 cm^{-1} (G-band) and 1334 cm^{-1} (D-band). The peak at 995 cm^{-1} is due to the stretching vibration of double bond vanadium and oxygen atoms,[28] and the peaks at 690 and 531 cm^{-1} correspond to V_2−O and V_3−O.[29] The stretching vibrations of V_2O_5 rods appear at the region of 409 and 286 cm^{-1} for VO and 486 cm^{-1} for V_3−O.[30]

XPS Studies. Figure 8 shows the XPS spectra of the G-V_2O_5 nanocomposite. The binding states of V_2O_5 rods embedded in the graphene sheets have been analyzed by the XPS studies. The survey spectrum (Figure 8(a)) shows the presence of all elements of the composite. The convolution spectrum of C 1s (Figure 8(b)) contains a peak at 284.47 eV due to the binding state of C═C in the nanocomposite. Figure 8(c) shows the spectrum for O 1s, which has two peaks at the binding energies of 530.69 and 531.55 eV, respectively. The peak at 530.69 eV corresponds to the bonded oxygen either in the V_2O_5 lattice or in graphene, and the peak at 531.55 eV has been assigned to the oxygen of carboxyl and hydroxyl groups of graphene.[31] The core level spectrum of V 2p shown in Figure 8 (d) reveals the binding state of 2p electrons of V at 521.79 and 517.00 eV, corresponding to V 2p1/2 and V 2p3/2, respectively, which are in good agreement with the binding energy value of VO for pure orthorhombic structure. The reduced graphene oxide has residual functional groups like OH and COOH on the surface, which can form physical bonding with V_2O_5 rods.

Surface Area Analysis. The BET surface area nitrogen-adsorption desorption isotherm of the G-V_2O_5 nanocomposite is shown in Figure 9. It is the type IV isotherm. The surface area of the G-V_2O_5 nanocomposite is calculated to be 115 m^2/g.[32] The order of the hexagonal structure of graphene pores is blocked due to the presence of V_2O_5 rods in the nanocomposite. The pore volume of the nanocomposite was 0.138 cc/g with the pore size of 2.7366 nm as calculated by the BJH method.[33] An increase in the relative pressure isotherm of the G-V_2O_5 nanocomposite reveals sharp inflections into P/P_0,

DOI: 10.1021/acsami.5b02715
ACS Appl. Mater. Interfaces 2015, 7, 14905−14911

which is attributed to the capillary strengthening inside the homogeneous interlayer spacing.

Photocatalytic Degradation. The photocatalytic activity of the synthesized G-V_2O_5 nanocomposite was analyzed using MB dye under UV, visible, and direct sunlight irradiations as shown in Figure 10. The irradiation of UV light for different time intervals and the rate of degradation of MB dye was observed as shown in Figure 10 (a). Figure 10(b) shows the absorption spectra of the MB dye solution with the G-V_2O_5 nanocomposite under visible light irradiation for different time intervals. This result shows that visible light irradiated MB dye with the G-V_2O_5 nanocomposite solution was degraded quickly within 150 min compared to UV irradiation. Figure 10(c) shows the absorption spectra of MB dye solution with the G-V_2O_5 nanocomposite under direct sunlight irradiation for different time intervals. The dye degrades at a faster rate under sunlight (90 min) compared to UV and visible light sources as the sunlight has higher intensity. To demonstrate the influence of graphene on the photodegradation, the degradation of MB with pure V_2O_5 was studied under visible light. Figure 10 (d) shows the variation of C/C_0 with time for V_2O_5 and the G-V_2O_5 nanocomposite, where C_0 is the initial concentration of the dye solution, and C is the concentration of the dye solution with respect to the degradation time 't'. It is obvious from Figure 10 (d) that the rate of degradation was quite faster in the composite compared to pure V_2O_5 rods, which shows the beneficial impact of graphene on the photocatalytic performance of the composite. The photocatalytic activity of the composite prepared by the present method is higher than the graphene-V_2O_5 based composite prepared by the hydrothermal method.[34]

The kinetics of the degradation process was studied under various irradiation sources. The rate constant and half-life time of the reaction was calculated using the following relations (eqs 1 and 2) and tabulated in Table 1. It is observed that the rate constant of the degradation reaction was relatively higher and the half-life time of the reaction was less under sunlight compared to UV and visible light, which leads to the faster degradation of dye under sunlight

$$\ln(C/C_0) = -kt \quad (1)$$

$$t_{1/2} = \ln 2/k \quad (2)$$

where 't' is the degradation time, and k is the rate constant of the degradation process.

The mechanism of photodegradation of the dye molecule due to the G-V_2O_5 composite under sunlight is shown in Figure 11.

The chemically reduced graphene has several residual functional groups like hydroxyl and carboxyl groups enriched on the surface. During the light irradiation, the excitons are generated in the V_2O_5 by absorbing the photons. The photoexcited electrons react with the residual functional groups of graphene and increase the oxide radicals ($O_2^{\bullet}$) by the reduction process at the conduction band. Moreover, the presence of graphene reduces the recombination of electrons and increases the reduction reaction as it is a highly conducting medium. At the same time, the oxidation reaction at the valence band increases the hydroxyl radicals ($OH^{\bullet}$) as shown in Figure 11. The $O_2^{\bullet}$ and $OH^{\bullet}$ radicals are highly active and decompose the dye molecules by the strong reaction. Therefore, the G-V_2O_5 nanocomposite exhibit enhanced photocatalytic activity compared to pure V_2O_5 rods.

CONCLUSION

The G-V_2O_5 nanocomposite has been successfully synthesized by a simple and efficient solution mixing method. Distribution of V_2O_5 rods on the graphene sheet was confirmed by SEM, HR-TEM, and XPS analysis. The XRD studies confirm the hexagonal and orthorhombic structure of the G-V_2O_5 composite. The XPS analysis confirmed the binding nature of VO with graphene sheets. The degradation of the MB dye solution was studied by irradiation with different light sources using the G-V_2O_5 nanocomposite as a catalyst. The results demonstrate that G-V_2O_5 acts as an efficient catalyst for the degradation of MB dye with various light sources. Among the different sources, the complete degradation of the dye was achieved within 90 min for the irradiation with direct sunlight.

AUTHOR INFORMATION

Corresponding Author

*Phone: 91-44-22359112. E-mail: rjvel@annauniv.edu.

Notes

The authors declare no competing financial interest.

ACKNOWLEDGMENTS

This research was supported by King Saud University, Deanship of Scientific Research, College of Science, Research Center. The authors would like to thank Shizuoka University, Hamamatsu Campus Center for Instrumental Analysis, Dr. M. Arivanandhan and Prof. Y. Hayakawa, Research Institute of Electronics, Shizuoka University, Japan for their help in the characterization.

REFERENCES

(1) Legrini, O.; Oliveros, E.; Braun, A. M. Photochemical processes for water treatment. *Chem. Rev.* **1993**, *93*, 671−698.

(2) Mills, A.; Davies, R. H.; Worsley, D. Water purification by semiconductor photocatalysis. *Chem. Soc. Rev.* **1993**, *22*, 417−425.

(3) Choudary, B. M.; Mahendar, K.; Kantam, M. L.; Ranganath, K. V. S.; Athar, T. The One-Pot Wittig Reaction: A Facile Synthesis of α,β-Unsaturated Esters and Nitriles by Using Nanocrystalline Magnesium Oxide. *Adv. Synth. Catal.* **2006**, *348*, 1977−1985.

(4) Dewangan, K.; Sinha, N. N.; Chavan, P. G.; Sharma, P. K.; Pandey, A. C.; More, M. A.; Joag, D. S.; Munichandraiah, N.; Gajbhiye, N. S. Synthesis and characterization of self-assembled nanofiber-bundles of V_2O_5: their electrochemical and field emission properties. *Nanoscale* **2012**, *4*, 645−651.

(5) Wu, M. C.; Lee, C. S. Field emission of vertically aligned V_2O_5 nanowires on an ITO surface prepared with gaseous transport. *J. Solid State Chem.* **2009**, *182*, 2285−2289.

(6) Novoselov, K. S.; Geim, A. K.; Morozov, S. V.; Jiang, D.; Zhang, Y.; Dubonos, S. V.; Grigorieva, I. V.; Firsov, A. A. Electric Field Effect in Atomically Thin Carbon Films. *Science* **2004**, *306*, 666−669.

(7) Zhang, J.; Xiong, Z.; Zhao, X. S. Graphene-metal−oxide composites for the degradation of dyes under visible light irradiation. *J. Mater. Chem.* **2011**, *21*, 3634−3640.

(8) Hu, C.; Lu, T.; Chen, F.; Zhang, R. A brief review of graphene−metal oxide composites synthesis and applications in photocatalysis. *J. Chin. Adv. Mater. Soc.* **2013**, *1*, 21−39.

(9) Shanmugam, M.; Alsalme, A.; Alghamdi, A.; Jayavel, R. Photocatalytic properties of Graphene-SnO_2-PMMA nanocomposite in the degradation of methylene blue dye under direct sunlight irradiation. *Mater. Express* **2015**, *5*, 319−326.

(10) Stengl, V.; Bakardjieva, S.; Grygar, T. M.; Bludska, J.; Kormunda, M. TiO_2-graphene oxide nanocomposite as advanced photocatalytic materials. *Chem Cent. J.* **2013**, *7*, 1−12.

(11) Liu, X.; Pan, L.; Zhao, Q.; Lv, T.; Zhu, G.; Chen, T.; Lu, T.; Sun, Z.; Sun, C. UV-assisted photocatalytic synthesis of ZnO−reduced

DOI: 10.1021/acsami.5b02715
ACS Appl. Mater. Interfaces 2015, 7, 14905−14911

graphene oxide composites with enhanced photocatalytic activity in reduction of Cr(VI). *Chem Eng. J.* **2012**, *183*, 238−243.
(12) Tan, L. L.; Ong, W. J.; Chai, S. P.; Mohamed, A. R. Reduced graphene oxide-TiO_2 nanocomposite as a promising visible-light-active photocatalyst for the conversion of carbon dioxide. *Nanoscale Res. Lett.* **2013**, *8*, 1−9.
(13) Chang, H.; Wu, H. Graphene-based nanocomposites: preparation, functionalization, and energy and environmental applications. *Energy Environ. Sci.* **2013**, *6*, 3483−3507.
(14) Qiu, B.; Zhou, Y.; Ma, Y.; Yang, X.; Sheng, W.; Xing, M.; Zhang, J. Facile synthesis of the Ti3(+) self-doped TiO_2-graphene nanosheet composites with enhanced photocatalysis. *Sci. Rep.* **2015**, *5*, 1−5.
(15) Weckhuysen, B. M.; Keller, D. E. Chemistry, spectroscopy and the role of supported vanadium oxides in heterogeneous catalysis. *Catal. Today* **2003**, *78*, 25−46.
(16) Martha, S.; Das, D. P.; Biswal, N.; Parida, K. M. Facile synthesis of visible light responsive V_2O_5/N, S−TiO_2 composite photocatalyst: enhanced hydrogen production and phenol degradation. *J. Mater. Chem.* **2012**, *22*, 10695−10703.
(17) Reddy, Ch. V. S.; Mho, S. I.; Kalluru, R. R.; Williams, Q. L. Hydrothermal synthesis of hydrated vanadium oxide nanobelts using poly (ethylene oxide) as a template. *J. Power Sources* **2008**, *179*, 854−857.
(18) Chen, D.; Yi, R.; Chen, S.; Xu, T.; Gordin, M. L.; Lv, D.; Wang, D. Solvothermal synthesis of V_2O_5/graphene nanocomposites for high performance lithium ion batteries. *Mater. Sci. Eng., B* **2014**, *185*, 7−12.
(19) Pham-Cong, D.; Ahn, K.; Hong, S. W.; Jeong, S. Y.; Choi, J. H.; Doh, C. H.; Jin, J. S.; Jeong, E. D.; Cho, C. R. Cathodic performance of V_2O_5 nanowires and reduced graphene oxide composites for lithium ion batteries. *Curr. Appl. Phys.* **2014**, *14*, 215−221.
(20) Thangappan, R.; Kalaiselvam, S.; Elayaperumal, A.; Jayavel, R. Synthesis of graphene oxide/vanadium pentoxide composite nanofibers by electrospinning for supercapacitor applications. *Solid State Ionics* **2014**, *268*, 321−325.
(21) Shanmugam, M.; Jayavel, R. Synthesize of Graphene-Tin Oxide Nanocomposite and Its Photocatalytic Properties for the Degradation of Organic Pollutants Under Visible Light. *J. Nanosci. Nanotechnol* **2015**, *15*, 7195−7201.
(22) Xiao, X.; Cheng, H.; Dong, G.; Yu, Y.; Chen, L.; Miao, L.; Xu, G. A facile process to prepare one dimension VO_2 nanostructures with superior metal−semiconductor transition. *CrystEngComm* **2013**, *15*, 1095−1106.
(23) Chan, C. K.; Peng, H.; Twesten, R. D.; Jarausch, K.; Zhang, X. F.; Cui, Y. Fast, Completely Reversible Li Insertion in Vanadium Pentoxide Nanoribbons. *Nano Lett.* **2007**, *7*, 490−495.
(24) Savariault, J. M.; Lafargue, D.; Parize, J. L.; Galy, J. Intercalation chemistry in layered transition metal oxide structures: Pyridine vanadium pentoxide. *J. Solid State Chem.* **1992**, *97*, 169−178.
(25) Tuinstra, F.; Koenig, J. L. Raman spectrum of graphite. *J. Chem. Phys.* **1970**, *53*, 1126−1130.
(26) Saito, R.; Hofmann, M.; Dresselhaus, G.; Jorio, A.; Dresselhaus, M. S. Raman spectroscopy of graphene and carbon nanotubes. *Adv. Phys.* **2011**, *60*, 413−550.
(27) Zhai, T.; Liu, H.; Li, H.; Fang, X.; Liao, M.; Li, L.; Zhou, H.; Koide, Y.; Bando, Y.; Golberg, D. Centimeter-Long V_2O_5 Nanowires: From Synthesis to Field-Emission, Electrochemical, Electrical Transport, and Photoconductive Properties. *Adv. Mater.* **2010**, *22*, 2547−2552.
(28) Sanchez, C.; Livage, J.; Lucazeau, G. Infrared and Raman study of amorphous V_2O_5. *J. Raman Spectrosc.* **1982**, *12*, 68−72.
(29) Yan, B.; Liao, L.; You, Y.; Xu, X.; Zheng, Z.; Shen, Z.; Ma, J.; Tong, L.; Yu, T. Single-Crystalline V_2O_5 Ultralong Nanoribbon Waveguides. *Adv. Mater.* **2009**, *21*, 2436−2440.
(30) Lee, S. H.; Cheong, H. M.; Seong, M. J.; Liu, P.; Tracy, C. E.; Mascarenhas, A.; Pitts, J. R.; Deb, S. K. Raman spectroscopic studies of amorphous vanadium oxide thin films. *Solid State Ionics* **2003**, *165*, 111−116.
(31) Zhang, J.; Xiong, Z.; Zhao, X. S. Graphene-metal oxide composites for the degradation of dyes under visible light irradiation. *J. Mater. Chem.* **2011**, *21*, 3634−3640.
(32) Brunauer, S.; Emmett, P. H.; Teller, E. Adsorption of gases in multimolecular layers. *J. Am. Chem. Soc.* **1938**, *60*, 309−319.
(33) Barrett, E. P.; Joyner, L. G.; Halenda, P. P. The determination of pore volume and area distributions in porous substances. 1. Computations from nitrogen isotherms. *J. Am. Chem. Soc.* **1951**, *73*, 373−380.
(34) Rakkesh, R. A.; Durgalakshmi, D.; Balakumar, S. Nanostructuring of GNS-V_2O_5/TiO_2 Core/Shell Photocatalyst for Water Remediation Applications under Sun-light Irradiation. *RSC Adv.* **2015**, *5*, 18633−18641.

DOI: 10.1021/acsami.5b02715
ACS Appl. Mater. Interfaces 2015, 7, 14905−14911